Monte Carlo simulations of $(e,2e)$ experiments on solids

M. Vos
Electronic Structure of Materials Centre, Flinders University of South Australia, G. P.O. Box 2100, Adelaide S.A. 5001, Australia

M. Bottema
Department of Mathematics and Statistics, Flinders University of South Australia, G. P.O. Box 2100, Adelaide S.A. 5001, Australia and the Centre for Sensor Signal and Information Processing (CSSIP), Technology Park, S.A., Australia

(Received 4 December 1995)

We simulate the multiple scattering effects occurring in an $(e,2e)$ experiment for a free-electron solid. Realistic cross sections for elastic and inelastic scattering events are used, for all the electrons involved. The aim of this paper is to simulate a real $(e,2e)$ experiment, and investigate how the multiple scattering parameters used affect the relation between the electronic structure of the solid and the actually measured intensity. Good agreement is found, on a semiquantitiative level, between the simulations and the actual experiments. [S0163-1829(96)05632-9]

I. INTRODUCTION TO THE PROBLEM

In the last year a series of $(e,2e)$ experiments was published.[1–8] For an introduction to the $(e,2e)$ technique as applied to solids, see Ref. 9. In these kinematically complete coincidence experiments one tries to measure the spectral momentum density of valence electrons in solids. The experimental results show a very clear resemblance between the positions of maximum intensities as a function of binding energy ε and momentum $\mathbf{q}$, as measured and calculated. However, there is nonzero intensity for other $\varepsilon,\mathbf{q}$ combinations not predicted by the band-structure calculations. This intensity is not fully understood. One of the fortes of the $(e,2e)$ technique should be that it is not only able to measure the dispersion relation between ε and $\mathbf{q}$, but also the intensity for each $\varepsilon,\mathbf{q}$ combination can be directly related to the target electron wave function. For solids this quantitative interpretation of the data is hampered by the intensity away from the dispersing peaks. Belief in the capability of $(e,2e)$ to measure the amplitude of the wave function in momentum space (''wave-function mapping'') is based on the proven success of this technique for atoms and molecules.[10] In these gas-phase experiments the probability that an electron interacts with more than one molecule is extremely small and can be safely neglected. This is not the case for experiments on solids, with their much larger densities. In order to minimize this problem experiments are done at high energy (i.e., low elastic and inelastic scattering cross sections) and with extremely thin free-standing films ($\simeq$100 Å thick). Still multiple scattering effects cannot be avoided completely. The purpose of this work is to get a better understanding of their influence on the spectroscopic results obtained.

II. THE $(e,2e)$ TECHNIQUE WITHOUT MULTIPLE SCATTERING

If a beam of high-energy electrons strikes a target, some of these electrons will scatter from target electrons. The energy and momentum transferred by the impinging electron ejects the target electron. In an $(e,2e)$ measurement the scattered and ejected electrons are detected in coincidence. $(e,2e)$ spectroscopy, as described here, involves large momentum transfers that allow us to describe the collision between impinging and target electrons as a *binary* collision.

We choose atomic units (a.u.) setting $\hbar=1$, and thereby equating momenta and wave numbers (1 a.u. as a unit of length corresponds to 0.529 Å; 1 a.u. of momentum corresponds to 1.89 Å^{-1}). The label $\mathbf{p}$ will denote electron momenta as determined outside a molecule or crystal and $\mathbf{q}$ the real momentum of the electron to be ejected in the molecule or crystal immediately before the scattering event. Scattered and ejected electrons are detected *in coincidence* and analyzed for their energies and momenta (E_s and $\mathbf{p}_s$ for the slower of the two electrons, E_f and $\mathbf{p}_f$ for the faster one).

Comparing the momenta and energies of the scattered and ejected electrons with the momentum $\mathbf{p}_0$ and energy E_0 of the incident electron yields the magnitudes of the momentum and binding energy of the ejected electron *before* the collision. We thus determine the binding energy ε as

$$\varepsilon = E_0 - E_s - E_f . \tag{1}$$

At sufficiently high energies the incoming and outgoing electrons can be treated as plane waves and the momentum of the target electron before the collision is given by

$$\mathbf{q} = \mathbf{p}_s + \mathbf{p}_f - \mathbf{p}_0 . \tag{2}$$

A complete description of the kinematics of each ionizing event is thus obtained. Moreover, for high energies of the incoming and outgoing particles the measured intensity is proportional to the spectral momentum density $|\phi(\varepsilon,\mathbf{q})|^2$ with $\phi(\varepsilon,\mathbf{q})$ the electron wave function in momentum space. This direct relation between the measured intensity and the wave function is an outstanding property of the $(e,2e)$ technique and for this reason it is often referred to as electron momentum spectroscopy.

The standard experimental configuration is shown in Fig. 1. Achieving sufficient momentum and energy resolution requires a well collimated monoenergetic electron beam impinging on a target. The incoming electron beam has an en-

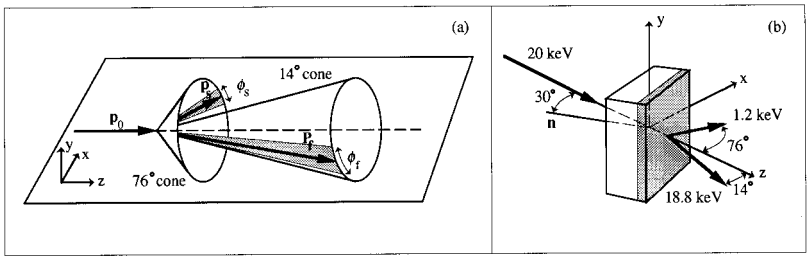

FIG. 1. A sketch of the experimental geometry of the $(e,2e)$ experiments. In (a) we show the range of angles measured. In (b) the usual sample orientation is shown. Most information is obtained from the shaded area of the sample, due to the small mean free path of the slow electron in this experiment.

ergy of 20 keV. The two detectors are positioned at angles of 14° (fast electron detector) and 75.6° (slow electron detector) with respect to the incoming beam. The energies of the detected electrons are $\simeq$18 800 and $\simeq$1200 eV, respectively. Both detectors accept electrons emerging from the target over part of a cone ($\pm 10°$ for the fast electron detector, $\pm 6°$ for the slow one). Under these conditions the sum of the momenta of the slow and fast electron equals the momentum of the incoming one, if all three electron trajectories (the incoming and the two outgoing ones) are in the same plane. If this is not the case then the momentum deficit $\mathbf{q}$ as calculated from Eq. (2) is directed approximately along the y axis. Thus, if one neglects multiple scattering effects one can associate the measured intensity $\mathcal{J}(\varepsilon,\mathbf{q})=\mathcal{J}(\varepsilon,0,q_y,0)$ with $|\phi(\varepsilon,0,q_y,0)|^2$.

III. $(e,2e)$ SPECTROSCOPY WITH MULTIPLE SCATTERING

A. Introduction

The previous description of the $(e,2e)$ process in solids is an oversimplification. It just assumes that the momentum and energy of the incoming and outgoing electrons as determined outside the solid are equal to the ones in the solid at the moment of the $(e,2e)$ event. Even for the thinnest film ($\simeq$10 nm) this assumption is only true for a small minority of the $(e,2e)$ events.

There are certain analogues with photoemission experiments, measuring crystal momentum and these experiments, measuring real momentum. In both cases we have an ionization event (by photon absorption or electron scattering) and high-energy electrons traveling to the surface and escaping from the solid. In photoemission we have to deal with one electron only. From the extensive literature of photoemission we know that in principle we have to treat the whole process (excitation, propagation, and escape from crystal) as one process (one-step model, e.g., Ref. 12) but a three-step model as proposed originally by Berglund and Spicer,[13] treating these three processes as independent has often proven to be useful and is intuitively very simple. It is within a similar framework that we try to describe the $(e,2e)$ process.

The first step (excitation) will be very similar to the one for $(e,2e)$ spectroscopy of atoms and free molecules, and is well understood for the high momentum transfer limit.[10] All $(e,2e)$ experiments on solid targets mentioned above are well within this limit. The third step (refraction at the surface) will be relatively minor as the inner potential of the solid (10–25 eV relative to the vacuum level) is small compared to the keV energy of these particles. Thus only a full understanding of the second step seems to be necessary in order to compare quantitatively the measured spectra (dispersion relation *and* intensity) with theory. This paper is an attempt to model the ''second'' step for amorphous solids.

In $(e,2e)$ spectroscopy we have to deal with the incoming electron (propagation away from the surface) and the two outgoing electrons (propagating towards the opposite surface of the thin film). This seems to complicate the analysis in the case of $(e,2e)$ spectroscopy. However, the kinetic energies of the electrons involved in the $(e,2e)$ experiments of solids (1 keV and up) are much higher than those in angle-resolved photoemission (tens of eV typically) and therefore the interaction of the electrons with the solid is much smaller. Because the energies are high, the electrons will (on average) travel a long distance (many interatomic distances) without scattering (deflection and/or energy loss). Because the scattering cross sections are reasonably well known, we can calculate these average distances between scattering events, i.e., the elastic and inelastic mean-free paths. Using Monte Carlo procedures, we try to get an impression of the frequency at which certain energy loss and momentum transfer combinations occur and we derive how these events will affect the measured $(e,2e)$ intensity.

There have been two other attempts to address (part of) this problem for $(e,2e)$ spectroscopy. Jones and Ritter tried a deconvolution approach of their $(e,2e)$ data.[11] Because of the state of the art of $(e,2e)$ at that time, their data had poor resolution and large error bars. A comparison of their deconvoluted data with the theory was not very conclusive. Allen *et al.*[14] and Matthews[15] focused on coherent elastic scattering of the electrons in a single crystal (Bragg reflections). Most of our experimental data are for amorphous and polycrystalline films. Indeed there are no obvious Bragg reflections visible in these experiments. $(e,2e)$ data of silicon single crystals have become available very recently and these data seem to show clear diffraction effects.[16] These single-crystal experiments are not discussed here. Monte Carlo simulations of the somewhat related problem of $(\gamma,e\gamma)$ spectroscopy have been published by Rollason and Woolf.[17]

B. Principle of calculation

Assume now a film with thickness T, and an $(e,2e)$ event occurring at depth t (see Fig. 2). The incoming electron travels over a distance $t_0=t/\cos\Theta_0$ before the collision occurs. Due to the possible occurrence of elastic and inelastic scattering the incoming energy E_0 and momentum $\mathbf{p}_0$ before striking the solid may change by ΔE_0 and $\Delta\mathbf{p}_0$. Similarly the outgoing slow [fast] electron travels a distance $t_s=(T-t)/\cos\Theta_s$ [$t_f=(T-t)/\cos\Theta_f$] and their initial energy decreases by ΔE_s (ΔE_f) and the momentum changes by $\Delta\mathbf{p}_s$ ($\Delta\mathbf{p}_f$). (Our detectors simultaneously measure a

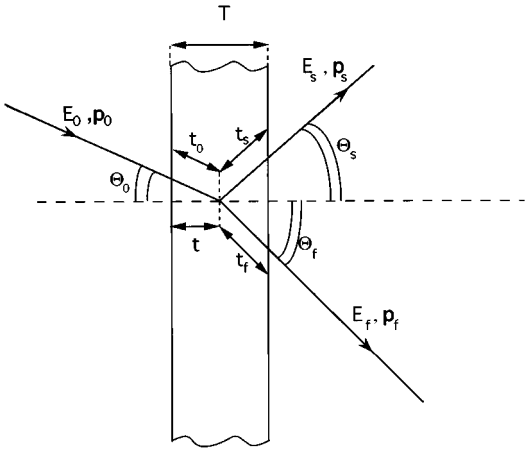

FIG. 2. Definition of the angles and distances used to describe the $(e,2e)$ event.

whole range of angles. The detected electron is analyzed, amplified by two channel plates, and detected on a resistive anode. From the ratio of the charge on all the four corners of the anode we calculate the exact momentum and energy of the detected particle (see Fig. 1). There are minor variations in length corresponding to the different trajectories. Also, as the detectors measure a range of energies, there is a small range of energy as well. We neglect these differences in angle and energy; i.e., we assume that the effects of elastic and inelastic scattering are the same for all electrons detected in a certain detector.)

If we include multiple scattering effects we cannot use the energy conservation equations (1) directly. Instead we measure the ''observed'' binding energy $\varepsilon_{\text{observed}}$:

$$\varepsilon_{\text{observed}} = E_0 - E_s - E_f, \tag{3}$$

with the actual binding energy of the electron ε given by

$$\varepsilon = \varepsilon_{\text{observed}} - \Delta\varepsilon^{\text{tot}}, \quad \text{with} \quad \Delta\varepsilon^{\text{tot}} = \Delta E_0 + \Delta E_s + \Delta E_f. \tag{4}$$

Similarly we have the ''observed'' momentum $\mathbf{q}_{\text{observed}}$:

$$\mathbf{q}_{\text{observed}} = \mathbf{p}_s + \mathbf{p}_f - \mathbf{p}_0, \tag{5}$$

which is related to the target electron momentum before ionization by

$$\mathbf{q} = \mathbf{q}_{\text{observed}} - \Delta\mathbf{p}^{\text{tot}}, \quad \text{with} \quad \Delta\mathbf{p}^{\text{tot}} = \Delta\mathbf{p}_0 + \Delta\mathbf{p}_s + \Delta\mathbf{p}_f. \tag{6}$$

Because of our experimental geometry $\mathbf{q}_{\text{observed}}$ is always directed along the y axis. As is clear from Eq. (6), target electrons with $\mathbf{q}$ directed away from the y axis may contribute to the measured intensity if $\Delta p_x^{\text{tot}} \neq 0$ or $\Delta p_z^{\text{tot}} \neq 0$.

One event without elastic scattering ($\Delta\mathbf{p}^{\text{tot}}=0$) and inelastic scattering ($\Delta\varepsilon^{\text{tot}}=0$) will be detected at an $(\varepsilon,\mathbf{q})$ combination where $|\phi(\varepsilon,\mathbf{q})|^2 \neq 0$. The sum of the contributions of all particles where both $\Delta\varepsilon^{\text{tot}}=0$ and $\Delta\mathbf{p}^{\text{tot}}=0$ would resemble the spectral momentum density $|\phi(\varepsilon,\mathbf{q})|^2$.

If only inelastic scattering events have occurred, the observed binding energy will be shifted to larger values by an amount $\Delta\varepsilon^{\text{tot}}$. Thus the contribution of all particles with this value of $\Delta\varepsilon^{\text{tot}}$ will resemble $|\phi(\varepsilon,\mathbf{q})|^2$ shifted by this amount to larger binding energies.

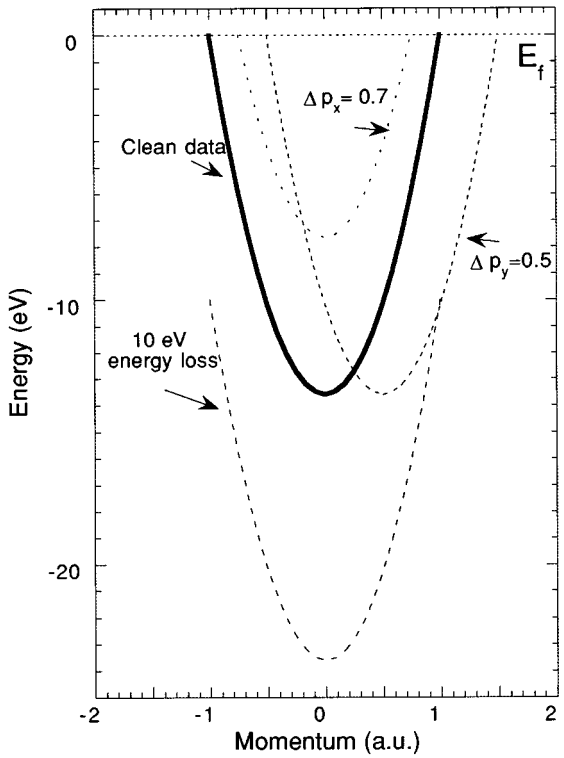

FIG. 3. Possible effects of multiple scattering on the measured dispersion relation. The events with no additional multiple scattering in any of the three trajectories involved will contribute to the intensity along the thick line. Those particles for which only inelastic multiple scattering occurred of say 10 eV will add to the intensity along the lower dotted line. Those particles that experience elastic scattering in the y direction will contribute to the intensity along the dispersion curve shifted by 0.5 a.u. If scattering occurs causing a momentum shift along the x (or equivalently the z) direction it will cause intensity along a line shifted upwards relative to the clean data.

In Fig. 3 we illustrate the effects for the case of a free-electron solid. The dispersion relation is for this case

$$\varepsilon_q = \varepsilon_0 - |q|^2/2m^*, \tag{7}$$

where ε_0 is the Fermi energy of the solid and m^* the effective mass of the electron. Only the states with positive binding energy will be occupied. The spectral momentum density is given by

$$|\phi(\varepsilon,\mathbf{q})|^2 = c\,\delta(\varepsilon - \varepsilon_q), \tag{8}$$

where c is a normalization constant. (Away from the Brillouin zone boundaries this is a useful starting point for most solids.)

If only elastic scattering events have occurred the situation is a little more complicated than the energy loss case, because of the vector nature of $\mathbf{p}$. If $\Delta\mathbf{p}^{\text{tot}}=(0,\Delta p_y,0)$ the measured parabola will be shifted along the momentum axis and has its minimum $\Delta\mathbf{p}^{\text{tot}}$ away from zero momentum. If $\Delta\mathbf{p}^{\text{tot}}=(\Delta p_x,0,\Delta p_z)$, the measured dispersion curve (again

for a free-electron solid) will appear as $\varepsilon=\varepsilon_0-[(\Delta p_x)^2+q_y^2+(\Delta p_z)^2]/2m^*$ instead of $\varepsilon=\varepsilon_0-q_y^2/2m^*$; i.e., the curve is shifted along the energy axis by $[(\Delta p_x)^2+(\Delta p_z)^2]/2m^*$. Examples of the effects of the different possible multiple scattering types are shown in Fig. 3. Of course, combinations of these different types may occur as well (energy loss combined with momentum transfer in an arbitrary direction).

We put the simulated intensity in a two-dimensional array $\mathcal{I}(\varepsilon_{\text{observed}},q_{y\ \text{observed}})$. In principle we could select for each incoming electron a specific target momentum $\mathbf{q}$, calculate its binding energy $\varepsilon_{\mathbf{q}}$ according to Eq. (7), and if the momentum $\mathbf{q}_{\text{observed}}$ is directed along the y axis, increment the array element $\varepsilon_{\text{observed}},q_{y\ \text{observed}}$ by 1. This would be a very time consuming way of simulating a spectrum. In reality we assume that each simulated event represents a large number of electrons with this $\Delta\varepsilon^{\text{tot}},\Delta\mathbf{p}^{\text{tot}}$ combination. The contribution of this class of events will be a complete dispersion curve shifted by $\Delta\mathbf{p}^{\text{tot}},\Delta\varepsilon^{\text{tot}}$ as described above. Thus from the simulation of N $(e,2e)$ events (typically, $N=5000-10\,000$) we get the following estimate of the measured $(e,2e)$ intensity:

$$\begin{aligned}\mathcal{I}(\varepsilon_{\text{observed}},q_{y\ \text{observed}})&=\sum_{i=1}^{N}|\phi(\varepsilon_{\text{observed}}-\Delta\varepsilon_i^{\text{tot}},\mathbf{q}_{\text{observed}}-\Delta\mathbf{p}_i^{\text{tot}})|^2\\&=\sum_{i=1}^{N}|\phi(\varepsilon_{\text{observed}}-\Delta\varepsilon_i^{\text{tot}},-\Delta p_{xi}^{\text{tot}},\\&\quad\times q_{y\ \text{observed}}-\Delta p_{yi}^{\text{tot}},-\Delta p_{zi}^{\text{tot}})|^2.\end{aligned}\tag{9}$$

This quantity can be compared directly with the experimentally measured spectra.

C. Details of Monte Carlo procedure

There are many other (some much more sophisticated) Monte Carlo studies published about electron-solid interaction. See, for example, Refs. 18–20. Here we describe our method briefly. As we are, at this stage, mainly concerned with understanding the basic physics of the $(e,2e)$ spectra, rather than getting an accurate fit of these, our approach is somewhat rudimentary, especially as far as the energy loss part is concerned.

In the calculation the first random number generated R_1 is used to determine the depth t at which the $(e,2e)$ event occurs $(t=R_1T)$. (All random numbers are taken from a homogeneous distribution between 0 and 1, unless otherwise stated.) Now we have to simulate three trajectories for electrons with energy E_0, E_s, and E_f and trajectory length t_0, t_s, and t_f, respectively. This is a standard problem and the procedures followed for each of the trajectories are identical. We describe this procedure next, referring to the energy as E_x and the trajectory length as t_x (where x represents 0, s, or f). For the inelastic energy losses we consider only the plasmon excitation processes. An estimate of the inelastic mean free path λ_{pl} of an electron with energy E can be obtained using an expression derived by Quinn:[21]

$$\lambda_{\text{pl}}=\frac{2a_0E_x}{E_{\text{pl}}}\left(\ln\left[\frac{(E_F+E_{\text{pl}})^{1/2}-E_F^{1/2}}{E_x^{1/2}-(E_x-E_{\text{pl}})^{1/2}}\right]\right)^{-1},\tag{10}$$

with a_0 the Bohr radius and E_{pl} the (experimentally determined) energy of the plasmon.

For the elastic scattering we are especially interested in those events with small angle scattering. If an electron is deflected over a large angle it will have only a very small probability of causing a coincidence event. After a small angle deflection the electrons may still cause a coincidence, but the momentum cannot be inferred anymore from Eq. (2). Thus these small angle deflections are in a way more serious than the large angle ones. It is therefore important to use the right elastic cross section at forward angles. In this paper we treat elastic scattering in two different ways. The simplest way (used unless stated otherwise) assumes a screened Coulomb interaction, which allows (in the Born approximation) for a simple analytical expression for the cross section. A somewhat more sophisticated approach uses the actual (Hartree-Fock) wave function of the free atom[22] and calculates from this, in the Born approximation, the scattering cross section. The scattering cross section obtained in this way is larger for small momentum transfer (see Fig. 4). Instead of an analytical expression we store the cross section in a look up table. In the Born approximation, the differential cross section depends on the transferred momentum only. Thus we can use the same table for all three trajectories (but for each particle energy the same momentum transfer will correspond to different scattering angles and the integrated cross section σ_e depends on energy as well). From these atomic cross sections we obtain the elastic mean free path in the solid by

$$\lambda_e=\frac{1}{N\sigma_e}\tag{11}$$

with N the number of atoms per unit volume in the solid.

For each of the trajectories we treat elastic and inelastic events independently. For the inelastic events the depth t_{pl} at which plasmon excitation occurs is

$$t_{\text{pl}}=-\lambda_{\text{pl}}\ln(R_2).\tag{12}$$

If t_{pt} is larger than the length of the trajectory t the excitation will not take place. If excitation takes place we decrease the energy of the particle with the plasmon energy. The plasmon energy distribution is approximated by a Gaussian, centered at the mean plasmon energy. Both the width and the energy of the plasmon can be obtained from electron energy-loss spectroscopy data.[23] For each plasmon excitation the energy is selected by a random number R_3 taken from this distribution.

Now we consider the remaining length is $t-t_{\text{pl}}$. We calculate a new distance at which a plasmon is excited and see if this distance is smaller than the remaining length. If this is the case we reduce the particle energy by another plasmon quantum chosen from the same distribution. This process is repeated until the next scattering distance is larger than the remaining length.

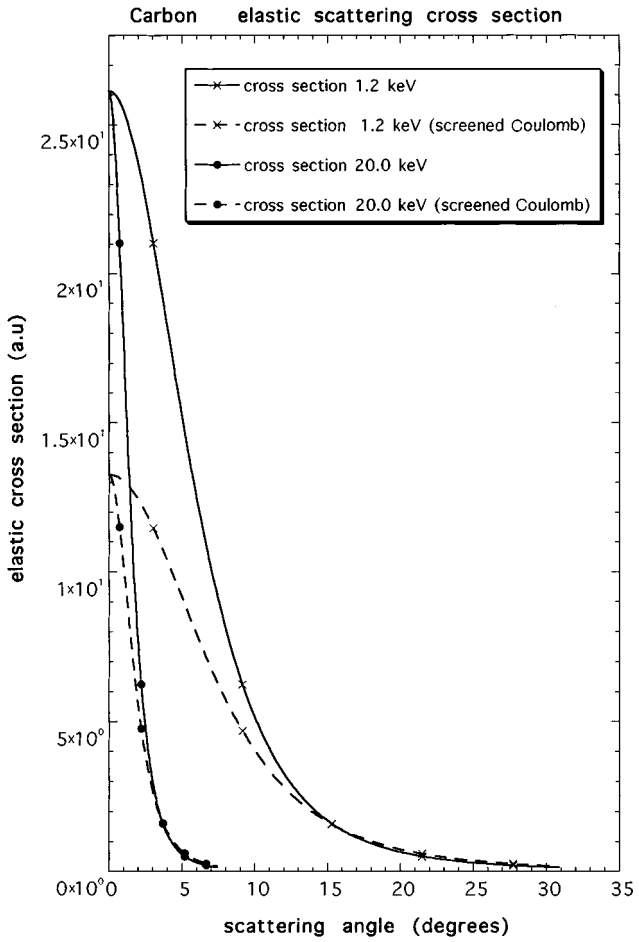

FIG. 4. The cross section derived in the Born approximation from either a screened Coulomb potential or from the actual atomic Hartree-Fock wave functions. The latter is considerably larger for small momentum transfer.

The elastic part is dealt with independently in a similar way. Again we determine the position of the first elastic scattering event:

$$t_e = -\lambda_e \ln(R_4). \tag{13}$$

If this distance is smaller than the trajectory length we determine the polar scattering from

$$R_5 = \frac{2\pi}{\sigma_e} \int_0^{\theta} \frac{d\sigma_e(E,\Theta)}{d\Omega} \sin\Theta d\Theta. \tag{14}$$

When we use a screened Coulomb potential we do this analytically (see Ref. 20), otherwise we use an array containing the integrated cross section (see Ref. 19). Finally the azimuthal angle is obtained from

$$\phi = 2\pi R_6. \tag{15}$$

Again this procedure is repeated until the next scattering event is beyond the remaining length of the trajectory.

After all three trajectories are simulated, all energy losses and momentum transfers are added and we increment the appropriate array elements simulating the measured intensity by 1 [see Eq. (9)].

IV. SIMULATION RESULTS

A. Energy-loss simulations

In these simulations, the energy-loss processes are treated in a very rudimentary way. The expected agreement can be estimated by comparing the simulated energy-loss spectra with the experimental ones. In these (noncoincident) measurements, the analyzer is at a large scattering angle (14° for the fast electron detector and 76° for the slow one.) We assume that elastic scattering occurs (from the nucleus, without significant energy transfer) at depth t (determined from a random number), and calculate the length of the incoming and outgoing trajectories and simulate the energy-loss processes as described above. The results are convoluted with 1 eV, the approximate resolution of these experiments. The results are displayed in Fig. 5 for carbon films of about 100 Å thick. These carbon films show a clear indication of the presence of two energy-loss structures the ''π'' plasmon around 6 eV and another loss feature around 25 eV. Only the latter was included in the simulations. Clearly the energy-loss processes are much more frequent for the slow electrons compared to the fast ones. The simulated data were convoluted with a Gaussian of 1 eV width. In the low-energy case

TABLE I. The expected number of clean $(e,2e)$ events for different spectrometer configurations. As an example a 100-Å-thick Al film was chosen as target. Also shown is the Mott cross section [i.e., the cross section for $(e,2e)$ events] for that scattering geometry. Clearly with higher energies and decreasing asymmetry the fraction of clean $(e,2e)$ events increases, but the cross section for $(e,2e)$ scattering decreases. [E_0, E_s, E_f, Θ_0, Θ_s, and Θ_f as defined in Fig. 2. N_{elastic}: the number of $(e,2e)$ events per 1000 *without* elastic scattering; N_{inelast}: the number of $(e,2e)$ events per 1000 *without* inelastic scattering; N_{none}: the number of $(e,2e)$ events per 1000 *without* either elastic or inelastic scattering; T_{average}: the average depth at which events without elastic and inelastic scattering occur, as measured from the surface facing the analyzers; cross section: the cross section for $(e,2e)$ events in arbitrary units.]

E_0 (keV)	E_s (keV)	E_f (keV)	Θ_0	Θ_s	Θ_f	N_{elastic}	N_{inelas}	N_{none}	T_{average} (angstrom)	Cross section
20	1.2	18.8	30	76	−14	58	177	32	4.5	11578
100	1.2	98.8	30	84	−6	86	214	63	6	12547
100	6	94	30	76	−14	380	595	262	27	1035
20	10	10	0	45	45	290	452	168	28	354
40	20	20	0	45	45	522	651	346	34	125
100	50	50	0	45	45	753	812	621	45	32

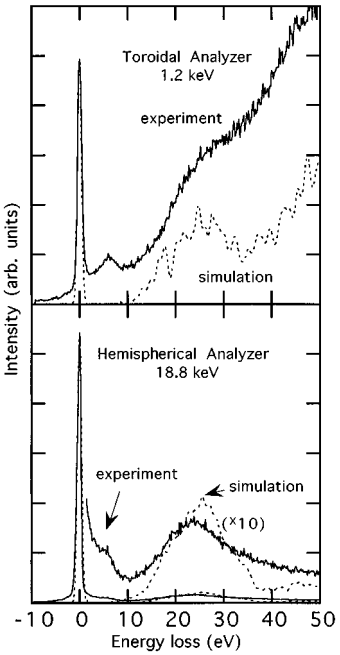

FIG. 5. The measured and simulated energy-loss spectra for a thin ≃100-Å annealed amorphous carbon film for the slow (1.2 keV) electron and the fast (18.8 keV) electron. The simulation only includes the main plasmon at 25 eV, but in the experiment there is also an indication of the π plasmon at around 6-eV energy loss.

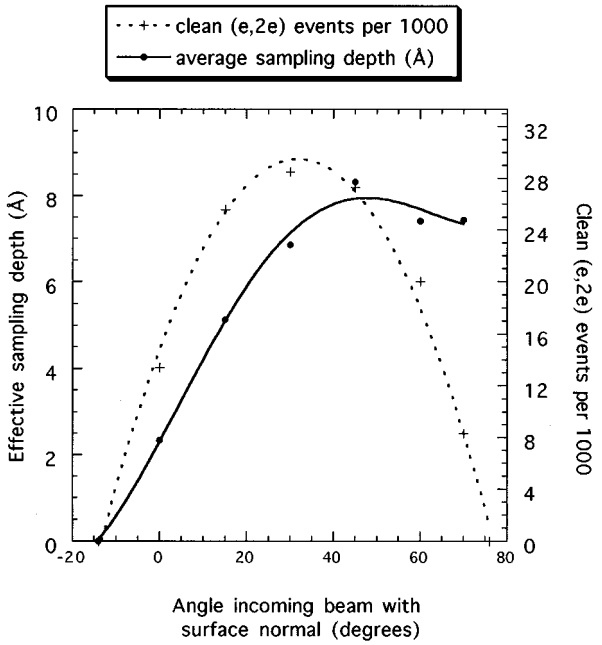

FIG. 6. The number of clean $(e,2e)$ events (i.e., no elastic or inelastic scattering) per 1000 incoming particles as a function of angle between the incoming beam and the surface normal. Also shown is the average depth (as measured from the surface facing the analyzers) of these clean events. Those configurations with the slow electron detector at a glancing angle are most surface sensitive. Optimum count rate is obtained around 30°.

(1.2 keV), we clearly underestimate the energy loss intensity. The agreement for the 18.8-keV electrons is better. Clearly the experimental zero loss peak (especially for the slow electron detector) is not too well described by a Gaussian distribution, its intensity falls off less quickly than the Gaussian with the same full width half maximum as the measured peak. Inclusion of these tails (by describing the line shape by a convolution of a Lorentzian and a Gaussian) would enhance the agreement somewhat. Thus we can only expect qualitatively correct simulations of the $(e,2e)$ measurements as far as the energy-loss features are concerned.

B. $(e,2e)$ spectroscopy: amount of valid data

Part of the spectrum of an $(e,2e)$ experiment will consist of events without additional energy losses and momentum transfer due to elastic scattering. Only these events are directly related to the target electron wave function. Thus, it is very important to maximize the number of these ''clean'' events. In Table I we give an overview of the number of clean events per 1000 incoming particles for the present geometry, and some other possible experimental configurations. Also displayed is the Mott cross section for $(e,2e)$, i.e., the likelihood that an $(e,2e)$ event will take place. In an ideal experiment one would like to optimize both cross section and the number of clean events. In practice, increase of one means a decrease of the other. In the present setup, the emphasis was on increasing the cross section. Clearly only a small fraction of the $(e,2e)$ events is not accompanied by energy losses and/or elastic scattering. Still it is possible to distinguish these clean events from the contaminated ones as the clean intensity is concentrated in very specific momentum–binding energy combinations. Another interesting parameter that can be simulated easily is the dependence of the number of clean events on the angle between the incoming beam and the surface normal, i.e., the effect of rotating the sample around the y axis of Fig. 1. The effect on the count rate is shown in Fig. 6. Clearly there is an optimum at ≃30°. In the same plot we show the average depth from which the clean events originate (as measured from the surface facing the analyzers). This depth is smaller for those configurations where the slow electron detector is at a glancing angle with the surface. This effect has been used to distinguish the surface contribution from the bulk one.[7]

C. $(e,2e)$ valence-band spectrum

The main aim is to compare the measured valence-band intensity with the simulated one. This is done for a highly oriented pyrolitic graphite (HOPG) sample. Details of sample preparation and measurement are given elsewhere.[2] The HOPG sample has a well defined c axis but is polycrystalline in the direction perpendicular to this axis. The y axis of the experiment is perpendicular to the c axis of the crystal. This has as a consequence that (in first approximation, without multiple scattering) the π electrons do not contribute. The main feature visible in the experiment is derived from the σ_1, σ_2, and σ_3 bands. This feature has roughly a parabolic shape, but does not extend all the way to the Fermi level. In the simulations we use a free-electron parabola with a Fermi energy equal to that of carbon. The resulting momentum densities are plotted as a function of binding energy (relative to the Fermi level) for both a simulation using a screened Rutherford cross section and a simulation using the

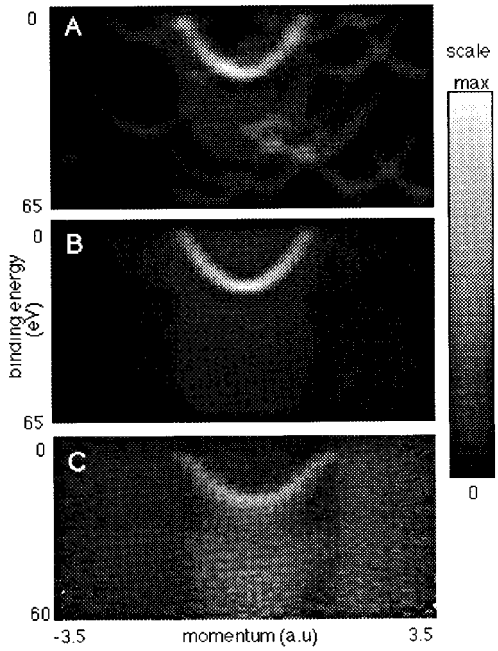

FIG. 7. In (a) we show a gray-scale plot the result for a carbon film simulated with 300 different $(e,2e)$ events. The parabolas derived from individual events are still clearly visible. In (b) we have a similar picture, but now for a simulation using 10 000 events. The distribution is now much more homogeneous, and only the clean $(e,2e)$ events stand out as a clear parabola. In (c) we have the experimental results of an actual experiment using a HOPG sample. It resembles the simulations in many ways.

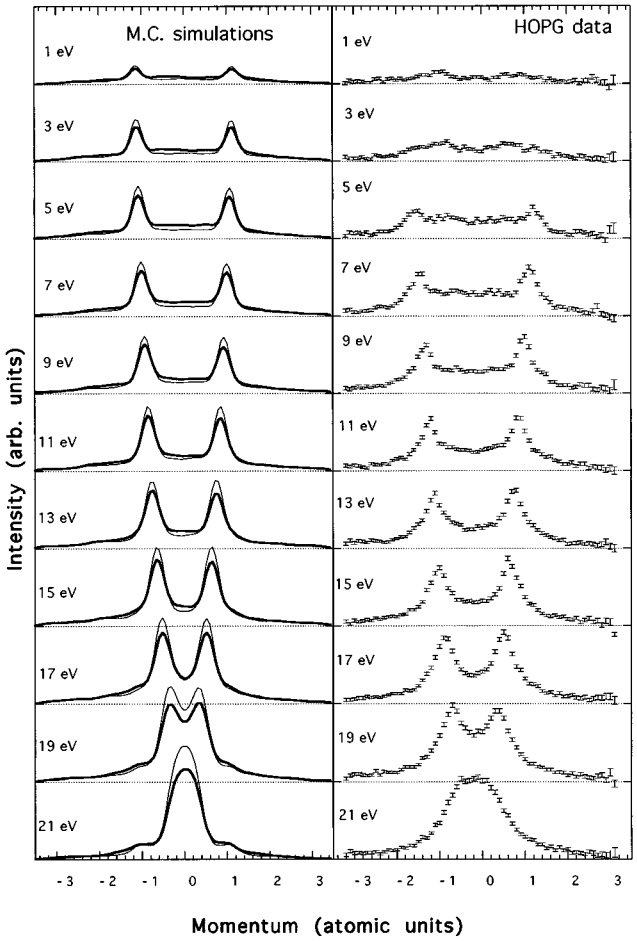

FIG. 8. The momentum densities for different binding energies as indicated. The left panel is for the simulated experiment. The thick line is for a simulation using cross sections derived from the Hartree-Fock wave functions, the thin line is for cross sections derived from a screened Coulomb potential. The latter one has more pronounced peaks in the simulation. The right panel shows the experimental data for HOPG. The general features of the experiment are very well reproduced by the simulation.

wave-function-derived cross section. We show in Fig. 7 the result of a simulation run using 300 and 10 000 particles as a grey-scale picture using the wave-function-derived cross section. In the case of 300 particles we can still recognize the individual parabolas corresponding to different events. For the one with better statistics the distribution is fairly smooth. Clearly visible is the intensity related to the clean events, and that related to multiple scattering. A more quantitative comparison with experiment can be made more easily from the plot of the measured and simulated dispersion curves. This is done in Fig. 8. The resemblance between simulation and experiment is, for the rough model used, surprisingly good. In particular the intensity in between the two dispersing peaks is reproduced nicely. The simulations were done both for the cross section derived from the screened Rutherford potential, and for the wave-function-derived cross section. For the first case the ratio of the intensity between the dispersing peak and the intensity of the peaks itself is somewhat lower, as expected because its cross section is smaller at forward angles. The wave-function-derived cross section seems to reproduce the experimental data somewhat better.

In the simulations we convolve the simulated intensity with an energy resolution of 4 eV and a momentum resolution of 0.3 a.u. There are some sharper features in the measured data [e.g., the core level of carbon has an experimental width of $\simeq$2 eV (Ref. 3)] so we think that part of this width is due to the sample, rather than spectrometer resolution. Things like lifetime broadening or surface effects may contribute to the width as well.

D. $(e,2e)$ spectrum over a larger energy range

A large number of $(e,2e)$ events are accompanied by more than one plasmon excitation. In the experiment this gives rise to a background extending all the way down to the carbon 1s core level (285 eV). This background was studied in some detail.[24] It was found that the momentum distribution increases in width with increasing energy loss. It was argued that large energy-loss events are due to $(e,2e)$ events taking place at small depth (t), i.e., with a large length of the slow trajectory t_s. This electron has the shortest mean free path (both elastic and inelastic) and thus multiple plasmon creation will be usually accompanied by multiple elastic scattering. In Fig. 9 we show the measured intensity integrated over momentum from -3 to 3 a.u. together with the results from the simulation. Clearly, the simulation drops off somewhat too quickly as could be expected since the slow electron energy-loss intensity (see Fig. 5) is too small. Still, considering the approximations made, the agreement is reasonable. Also interesting is the comparison of the momentum distribution of the measurement and simulation as a function

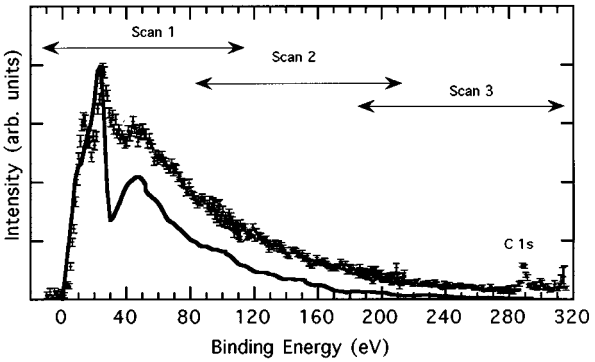

FIG. 9. The measured intensity for an annealed amorphous carbon film over a wide energy range. The spectrum is constructed of three scans with a fair overlap. Around 285 eV we see the small contribution of the carbon 1*s* level. The solid line is the result of a computer simulation. It seems to decay somewhat faster than the experimental spectrum (the 1*s* level was not incorporated in the simulations).

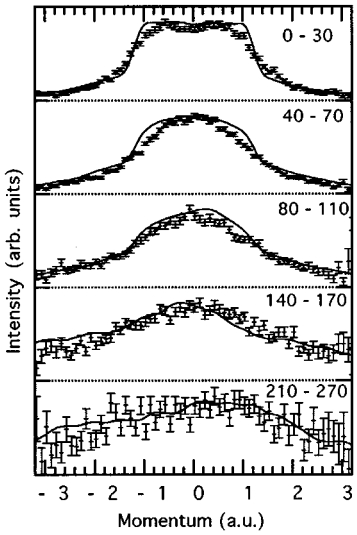

FIG. 10. The development of the momentum distribution of the tail of a carbon valence-band spectrum with increasing energy loss. With increasing energy loss both the simulated and the measured spectrum broaden in a very similar way. Each panel is normalized to equal height for easy comparison.

of energy loss. This is done in Fig. 10. For more easy comparison, the heights of the distributions are scaled to equal height in each panel. Both the simulated and measured momentum densities broaden with increasing energy loss, in a surprisingly similar fashion.

V. CONCLUSION

In this paper we describe a Monte Carlo approach to the interpretation of $(e,2e)$ data. We treat the elastic and inelastic scattering independently. The elastic scattering is taken to be completely incoherent in this approach. As far as inelastic scattering is concerned, only plasmon losses are considered. The simulations are done without adjustable parameters, all input to the program is derived from theoretical estimates of the interactions. It is surprising that within this framework it is possible to describe the $(e,2e)$ data semiquantitatively; i.e., we reproduce all the striking features of the spectra. The main deviations are probably due to (i) inaccuracy of the treatment of inelastic scattering, (ii) oversimplification of the model spectral momentum density used, and (iii) uncertainty in the thickness of the sample. This paper shows, however, that this type of approach of the description of $(e,2e)$ measurements is very promising and may develop into a fully quantitative description of $(e,2e)$ experiments. This would make quantitative tests of the electronic structures of materials possible, in the same way as has been done for the case of atoms and molecules.

ACKNOWLEDGMENTS

The authors want to thank the staff of the Electronic Structure of Materials Centre for their indispensable contributions to the $(e,2e)$ experiments and Ian McCarthy for providing us with the wave-function-derived cross section and for reading the manuscript carefully. The Electronic Structure of Materials Centre is supported by a grant of the Australian Research Council.

[1] P. Storer, S. A. C. Clark, R. C. Caprari, M. Vos, and E. Weigold, Rev. Sci. Instrum. **65**, 2214 (1994).
[2] M. Vos, P. Storer, S. A. Canney, A. S. Kheifets, I. E. McCarthy, and E. Weigold, Phys. Rev. B **50**, 5635 (1994).
[3] R. S. Caprari, S. A. C. Clark, I. E. McCarthy, P. Storer, M. Vos, and E. Weigold, Phys. Rev. B **50**, 12 078 (1994).
[4] M. Vos, P. J. Storer, Y. Q. Cai, I. E. McCarthy, and E. Weigold, Phys. Rev. B **51**, 1866 (1995).
[5] Y. Q. Cai, M. Vos, P. Storer, A. S. Kheifets, I. E. McCarthy, and E. Weigold, Phys. Rev. B **51**, 3449 (1995).
[6] M. Vos, P. Storer, Y. Q. Cai, A. S. Kheifets, I. E. McCarthy, and E. Weigold, J. Phys. Condens. Matter **7**, 279 (1995).
[7] M. Vos, S. A. Canney, P. J. Storer, I. E. McCarthy, and E. Weigold, Surf. Sci. **327**, 387 (1995).
[8] Y. Q. Cai, M. Vos, P. Storer, A. S. Kheifets, I. E. McCarthy, and E. Weigold, Solid State Commun. **95**, 713 (1995).
[9] M. Vos and I. E. McCarthy, Rev. Mod. Phys. **63**, 713 (1995).
[10] I. E. McCarthy and E. Weigold, Rep. Prog. Phys. **54**, 789 (1991).
[11] R. Jones and A. L. Ritter, J. Electron. Spectrosc. Relat. Phenom. **40**, 285 (1986).
[12] P. J. Feibelman and D. E. Eastman, Phys. Rev. B **10**, 4932 (1974).
[13] C. N. Berglund and W. E. Spicer, Phys. Rev. **136**, 1030A (1964).
[14] L. J. Allen, I. E. McCarthy, V. W. Maslen, and C. J. Rossouw, Aust. J. Phys. **43**, 453 (1990).
[15] R. Matthews, Ph.D. thesis, Flinders University of South Australia, 1993 (unpublished).
[16] S. Utteridge, Ph.D. thesis, Flinders University of South Australia, 1996 (unpublished).
[17] R. Rollason and M. B. J. Woolf, J. Phys. Condens. Matter **7**, 7939 (1995).
[18] R. Shimizu and Z.-J. Ding, Rep. Prog. Phys. **55**, 487 (1992).

[19] K. Tökési, A. Némethy, L. Kövér, D. Varga, and T. Mukoyama, J. Appl. Phys. **77**, 3763 (1996).
[20] M. Dapor, Phys. Rev. B **46**, 618 (1992).
[21] J. J. Quinn, Phys. Rev. **126**, 1453 (1962).
[22] E. Clementi and C. Roetti, At. Data Nucl. Data Tables **14**, 177 (1974).
[23] R. F. Eggerton, *Electron Energy Loss Spectroscopy* (Plenum, New York, 1986).
[24] M. Vos, P. Storer, A. S. Kheifets, I. E. McCarthy, and E. Weigold, J. Electron. Spectrosc. Relat. Phenom. **76**, 103 (1995).